J. Micromech. Microeng. 4 (1994) 192–204. Printed in the UK

Simulation of microfluid systems

Roland Zengerle and Martin Richter

Fraunhofer-Institut für Festkörpertechnologie, Hansastrasse 27 d, D-80686 Munich, Germany

Received 1 August 1994, accepted for publication 4 October 1994

Abstract. The dynamic behavior of microfluid devices like miniaturized diaphragm pumps, microvalves and flow channels will be discussed. Special interest is directed to the dynamics of microminiaturized diaphragm pumps. A formalism will be given, which allows the evaluation of the interaction between these pumps and the connected fluid system. The results of the simulation will be compared with transient pressure measurements on pneumatically and electrostatically actuated diaphragm pumps on the millisecond time scale. It will be outlined how the dynamic behavior of more complex fluid systems can be described. Hence the hydraulic simulation of chemical analysis systems, consisting of several micropumps, flow channels, sensing and mixing elements becomes possible in the future.

1. Introduction

In the development of micromachined physical, chemical and biological sensors worldwide advances have been made during the last few years [1]. In connection with this many fluidic components like miniaturized flow channels, active and passive check valves as well as miniaturized fluid pumps have been presented [2, 3]. With a combination of these elements, a lot of applications in chemical process control, medical drug delivery systems, environment control or industrial equipment are becoming possible. A first application was that miniaturized diaphragm pumps were integrated with flow sensors [4, 5]. This lead to an internal feedback system which allowed precise fluid control in the μl/min range, with smallest dead volumes and fast response times. Two micropumps and an ISFET-based sensor have been stacked together for the measurement of ion concentrations [6] and more complex systems will follow.

Until now little has been known about the dynamic interaction in micro fluid systems, consisting of pumps, valves, flow channels, elastic chambers and flow sensing elements. In the following paper the hydraulic part of these systems will be discussed. The procedure in the simulation of macroscopic hydraulic systems and networks can be adopted in many cases. In order to calculate the dynamics of a fluid system, the static and dynamic properties of the different components have to be specified. This covers the static flow characteristic, the static volume deformation, as well as the inertia effects of the single devices.

The behavior of most microminiaturized devices like flow channels, elastic chambers and passive check valves is very similar to their macroscopic equivalent. Other components like microminiaturized diaphragm pumps behave differently in the microscopic world. The different elements will be discussed below.

0960-1317/94/040192+13$19.50

2. Flow channels

In a miniaturized fluid system, different function elements have to be connected with flow channels. In the case of laminar flow in a circular pipe, the volume flow characteristic $\Phi(p)$ is given by the law of Hagen–Poiseuille

$$\Phi(p) = \frac{\pi R^4}{8\eta L} p \tag{1}$$

where R and L are radius and channel length, η and p are dynamic viscosity and hydrostatic pressure difference respectively. Often the cross sections of fluid channels in microminiaturized fluid systems are not circular. Then it is necessary to evaluate the flow characteristic from Navier–Stokes equation [7]. But also measurements can be carried out for the determination of the flow characteristic of fluid channels [8, 9].

In order to decide, whether the fluid flow through a miniaturized channel is laminar or turbulent, it is a common practise to calculate the Reynolds number Re and to compare the result with a transitional number of 1000–2500. The Reynolds number can be calculated as

$$\mathrm{Re} = \frac{R\rho u}{\eta} \tag{2}$$

where u is the average flow velocity in the flow channel and ρ is the density of the fluid. The Reynolds numbers are usually considerably smaller than the transitional number for channels in microminiaturized fluid systems. Therefore the microscopic flow through the channels can be assumed as laminar and the pressure dependence of the flow characteristic is linear. In this case equation (1) can be written as:

$$\Phi(p) = \frac{1}{\rho\beta} p \tag{3}$$

β can be seen as a fluid resistance [10].

The inertia of the fluid in flow channels also has to be regarded. In order to change an established volume flow through a fluid channel a pressure difference p_{inert} is needed. The pressure difference and the time dependent change in volume flow are connected via the equation (4)

$$p_{inert} = \rho\alpha\frac{d\Phi}{dt}. \quad (4)$$

The fluid inductivity α characterizes the ability of saving kinetic energy. Considering Newton's equation for inert and incompressible fluids in any tubes with a constant cross section $A_\square$ and length L, the fluid inductivity of a channel can be calculated as [10]

$$\alpha = \frac{L}{A_\square}. \quad (5)$$

As the hydrostatic pressures in miniaturized fluid systems are quite low, the volume deformation of fluid channels as well as the compressibility of the fluid can usually be neglected. So the basic properties of fluid channels in miniaturized fluid systems are given by the fluid resistance β and the fluid inductivity α.

3. Elastic components

In macroscopic hydraulic systems elastic components often are used as damping elements in order to smooth the pulsation in volume flow of reciprocating pumps. The same can be achieved in the microscopic world. If we consider incompressible fluids, the elastic components have to be characterised only by their pressure dependent volume deformation, which usually is called the fluid capacitance C [10].

$$C = \rho\frac{dV}{dp}. \quad (6)$$

In microfluids often a square membrane is used as capacitance. In this case, the fluid capacitance can be calculated as [11]:

$$C = \rho\frac{dV}{dp} = \frac{6\rho d^6(1-\nu^2)}{\pi^4 h^3 E} \quad (7)$$

The parameters d and h denote width and thickness of the membrane, E and ν are the Youngs modulus and the Poisson's ratio. It should be noted that the fluid capacitance becomes pressure dependent, if the deflection of the diaphragm is about the size of the thickness h. Usually the flow resistance β as well as the fluid inductivity α of elastic components are much smaller than the corresponding values of the connected fluid channels and so they can be neglected.

4. Microvalves

Passive check valves are important components of miniaturized fluid systems. They are used for example to direct the flow from inlet to outlet in miniaturized diaphragm pumps. Normally, passive check valves consist of two parts: a flexible diaphragm (or a flexible flap)

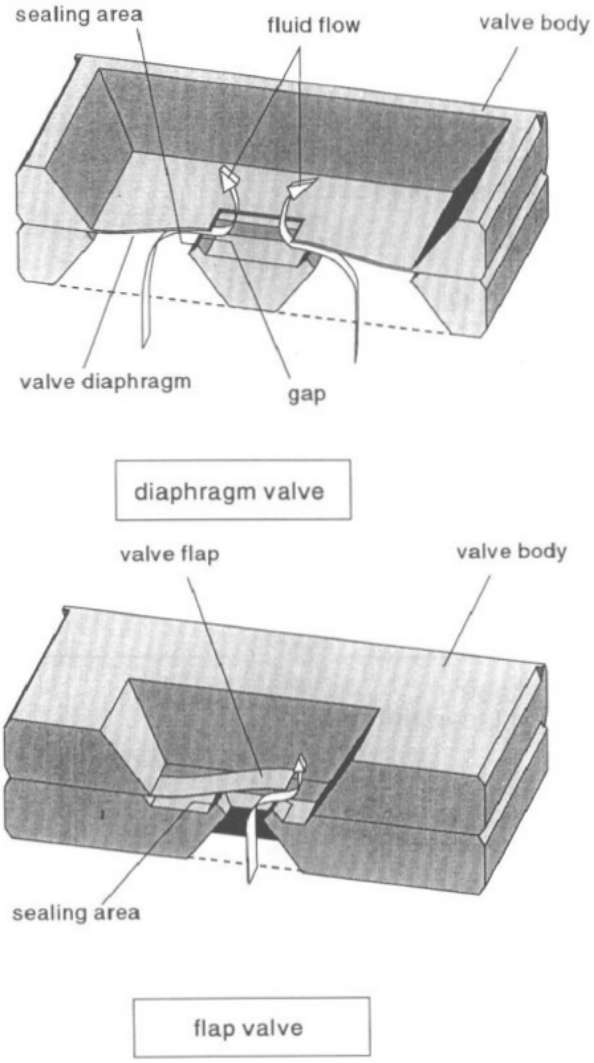

Figure 1. Cross section through different types of microminiaturized check valves [14].

and a sealing area (figure 1). If the hydrostatic pressure difference operates in forward direction (figure 2), the valve diaphragm opens, and fluid flow occurs. In real applications, microvalves can be leaky due to particles on the valve seat. Two characteristic functions are necessary in order to describe the valve operation: the flow characteristic and the volume displacement characteristic.

The flow characteristic of a microvalve is the result of two effects. First, the pressure dependent deformation of the diaphragm leads to a pressure dependent gap. If the shape of the gap is known, the microscopic flow through the gap can be calculated. From the theoretical point of view this can be done either by finite-element analysis or by approximate formulae. From the experimental point of view, the flow characteristic of microvalves can be recorded by measurements. Typical flow characteristic curves $\Phi(p)$ of passive check valves, made by micromachining of silicon, are depicted in figure 3(a). In many cases a very non-linear behaviour can be seen in forward direction. So it is impossible to define a constant fluid resistance β.

The volume displacement characteristic $V_{valve}(p)$ of passive check valves and thereby also the fluid capacitance of microvalves differs very much between forward and

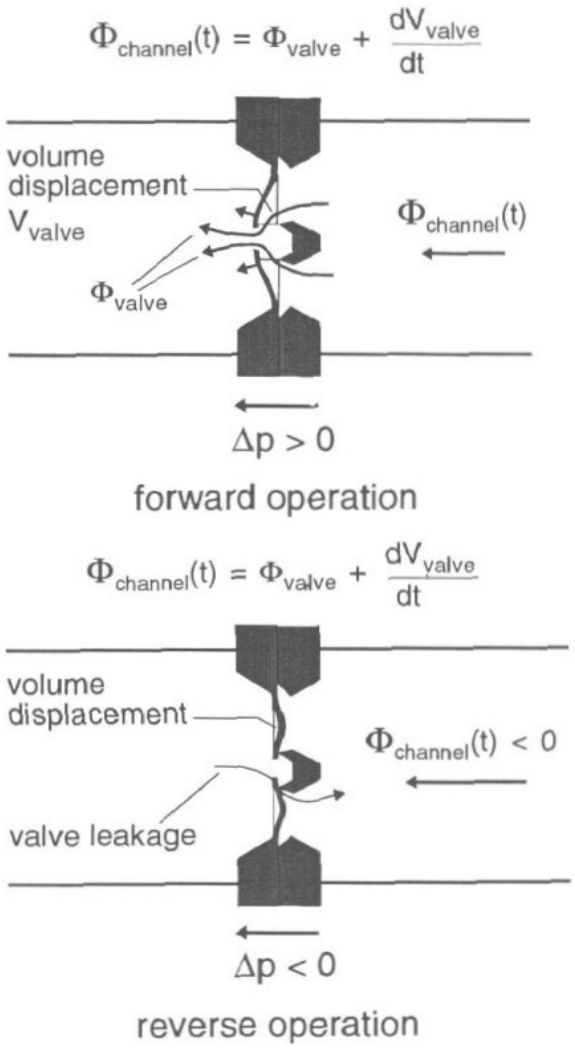

Figure 2. Forward and reverse operation of a passive check valve.

reverse direction. Not even the fluid capacitance in forward direction alone is constant (figure 3(b)).

For calculations following later on, it is important to know that the volume flow $\Phi(p)$ through the valve and the transient change (dV_{valve}/dt) in the volume displacement of the valve have to be added in order to get the volume flow in the fluid channel:

$$\Phi_{channel} = \Phi_{valve} + \frac{dV_{valve}}{dt}. \qquad (8)$$

As will be shown below, the inertial (inductivity) of the fluid in flow channels is important if hydrostatic pressure changes occur on the time scale of several milliseconds. Compared to this, the inertia (inductivity) of the movable valve parts can be neglected, because the resonance frequencies of these parts usually are in the range of 10 kHz. So inertia effects of microvalves only can be expected if hydrostatic pressure changes occur on the time scale of 100 μs. Therefore in a typical operation mode of micro fluid systems, the inertia of the microvalves is negligible (quasistatic behavior) compared to the inertia of the fluid.

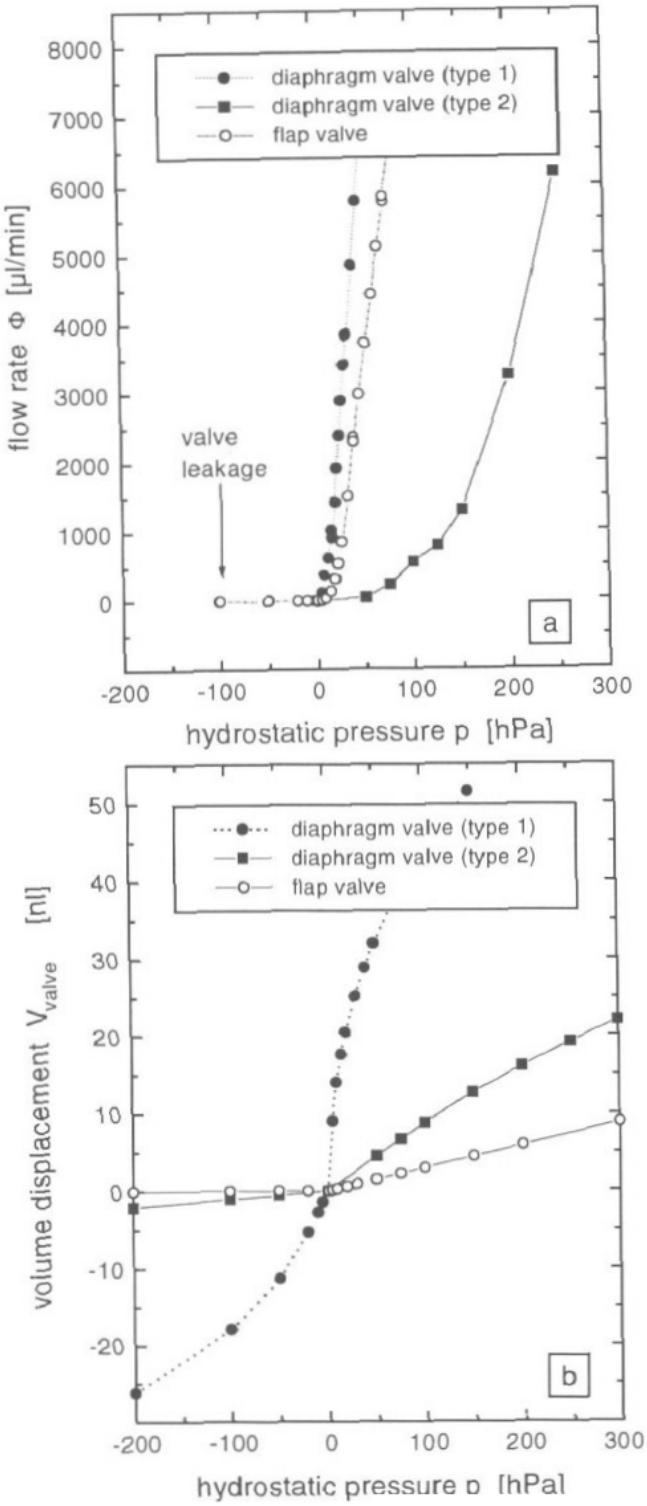

Figure 3. Flow characteristic and volume deformation of different types of microvalves [14]. The thickness of the valve diaphragm between type 1 and 2 varies by a factor of 1.7.

5. Miniaturized diaphragm pumps

Miniaturized diaphragm pumps are widely used as active components in microfluid systems. At first sight, the pumps resemble very much their macroscopic equivalents. They consist of an actuated pump diaphragm and two passive check valves. However, there is a large difference in

dynamic behavior between macroscopic and microscopic devices. The volume flow of the macroscopic reciprocating pump is given by the externally forced volume stroke V_H of a piston (or a diaphragm) and the operation frequency f:

$$\Phi = f V_H. \tag{9}$$

Considering macroscopic pumps, a coupling between the volume stroke of the piston and the other fluid parameters (for example the hydrostatic pressure difference between inlet and outlet side of the pump) can be neglected. But in the case of miniaturized diaphragm pumps, only the driving forces acting on the driving diaphragm and not the volume stroke of the driving diaphragm can be controlled by the operator. The volume stroke depends on the hydrostatic pressures at the inlet and outlet side of the pump, the operation frequency and the properties of the passive check valves. Microminiaturized diaphragm pumps therefore have to be handled as complex sub-systems in fluid networks.

For the development of a thermopneumatically actuated miniaturized diaphragm pump, a bond graph theory has been used to calculate the dynamic behavior [12]. The theoretical model of this pump describes the interaction between the fluid resistances and the fluid capacitances of the valves, the capacitance of the driving diaphragm and the thermopneumatic actuation system. We developed an analytical model for the description of miniaturized diaphragm pumps driven by different actuation mechanisms [13]. In the following we present this model, starting with the most basic description of a miniaturized diaphragm pump.

5.1. Basic model

The different components of miniaturized diaphragm pumps, usually two passive check valves and an actuated pump diaphragm, are depicted in figure 4. The dynamics of this model can be evaluated by the use of the continuity equation (10), which combines the mass flow into the pump chamber with the transient change in pump chamber content:

$$-\oint j \mathrm{d}S = \frac{\mathrm{d}m}{\mathrm{d}t} \tag{10}$$

If the inertia of the check valves can be neglected, the time dependent mass flow density j into the pump chamber is given by the static flow characteristic Φ_{iv} and Φ_{ov} of the two passive check valves.

$$-\oint j \mathrm{d}S = \rho\left(\Phi_{iv}(p_{iv}) - \Phi_{ov}(p_{ov})\right) \tag{11}$$

The static volume flow through the valves depends on the hydrostatic pressure differences at the inlet ($p_{iv} = p_1 - p$) and outlet ($p_{ov} = p - p_2$) valve. On the other hand, the time dependent change in mass inside the pump chamber can be calculated from the time dependent volume change of the elastic components. In the case of an incompressible fluid this results in:

$$\frac{\mathrm{d}m}{\mathrm{d}t} = \rho \frac{\mathrm{d}}{\mathrm{d}t}\left(V_0(p) + V_m(p, A) - V_{iv}(p_{iv}) + V_{ov}(p_{ov}) - V_{gas}(p)\right) \tag{12}$$

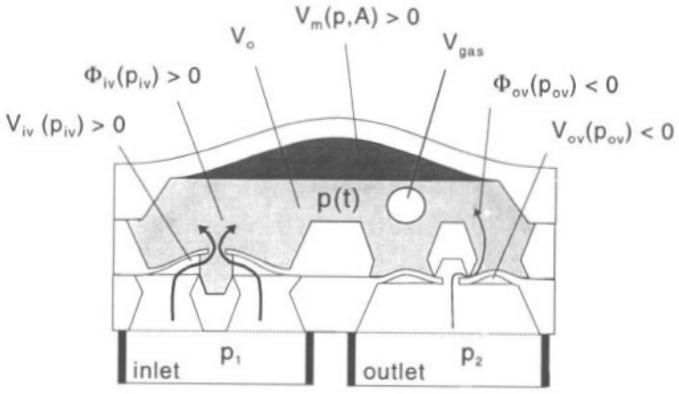

Figure 4. Schematic view of a microminiaturized diaphragm pump.

V_0, V_{iv} and V_{ov} are the total pump chamber volume, as well as the volume displacement of inlet and outlet valve respectively (see figure 4). The most important part of the equation (12) is given by the actuation characteristic $V_m(p, A)$ of the pump. $V_m(p, A)$ describes the coupling between the volume displacement of the driving diaphragm and the resulting pressure p inside the pump chamber at a specified actuation condition $A(t)$. In the case of an electrostatically or piezoelectrically actuated diaphragm pump, $A(t)$ corresponds with the electrical supply voltage $U(t)$. If on the other hand a pneumatically actuated diaphragm pump has to be calculated, $A(t)$ corresponds with the pneumatic actuation pressure $p_a(t)$.

The actuation characteristic $V_m(p, A)$ has to be calculated for the particular actuation mechanism, considering a static equilibrium between all forces acting on the diaphragm (quasistatic model). For pneumatic actuation this simply results in

$$V_m(p, A) = C_m(p - A) = C_m(p - p_a) \tag{13}$$

where C_m is the fluid capacitance of the driving diaphragm and $(p - p_a)$ is the resulting pressure acting on it. The actuation characteristic $V_m(p, A)$ and a typical time dependence of the actuation parameter $A(t)$ are depicted in figure 5. The corresponding functions for an electrostatically actuated diaphragm pump are given in figure 6. In this case the actuation characteristic shows a strong non-linear behavior. In area I this results from the contact between the driving diaphragm and the counterelectrode (see figure 6(a)). In area II the non-linear dependence between the attractive electrostatic forces and the local distance between the driving diaphragm and the counterelectrode results in the non-linear actuation characteristic [13].

The time dependence of the actuation parameter $A(t)$ is assumed to be fixed by the external operator (see figure 5(c) and 6(c)) and it is supposed that there is no feedback from the dynamics of the pump. In the case of electrostatic actuation, normally a square wave with variable frequency is used (figure 6(c)).

The insertion of the equations (11) and (12) in (10) results in the basic differential equation (14) for the evaluation of the time dependent pressure p inside the pump

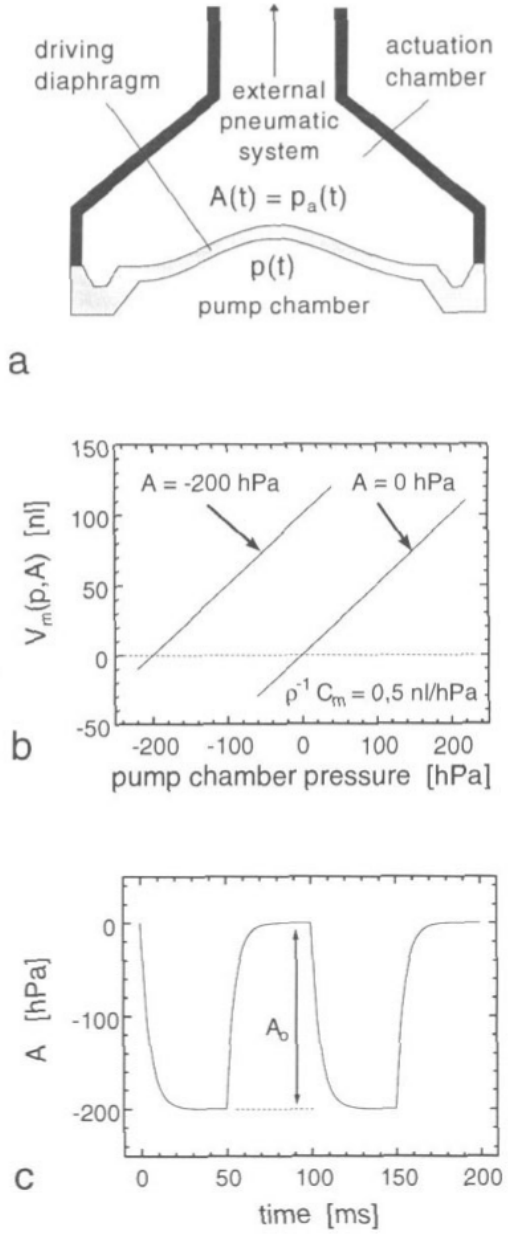

Figure 5. Schematic view (a), actuation characteristic (b) and transient actuation parameter (c) of a pneumatically driven actuation unit.

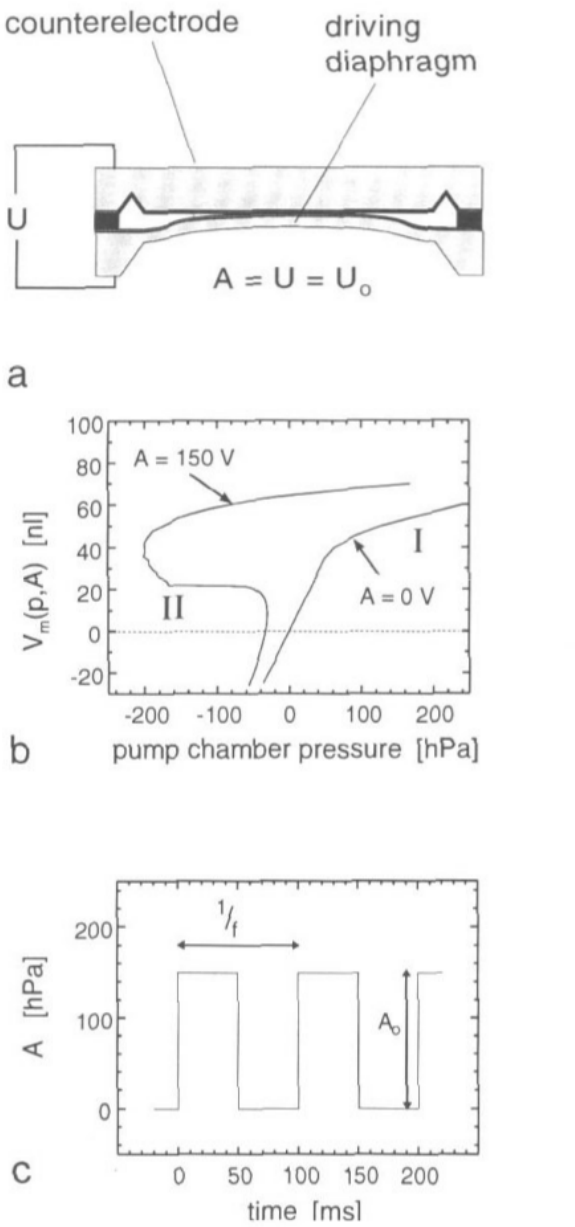

Figure 6. Schematic view (a), actuation characteristic (b) and transient actuation parameter (c) of an electrostatically driven actuation unit.

chamber:

$$\frac{dp}{dt} = \frac{\Phi_{iv}(p_{iv}) - \Phi_{ov}(p_{ov}) - \frac{\partial V_m}{\partial A}\big|_p \frac{dA}{dt}}{\frac{\partial V_m}{\partial p}\big|_A - \frac{dV_{iv}}{dp} + \frac{dV_{ov}}{dp} + \frac{dV_0}{dp} - \frac{dV_{gas}}{dp}}. \qquad (14)$$

Most often the flow resistances and fluid capacitances of microvalves are not constant and in some cases the actuation characteristic curve $V_m(p, A)$ is a strongly non-linear function (see figure 6(b)). Therefore, solving of equation (14) usually is only possible by numerical methods.

In equation (14) the fluid inductivity of flow channels has been neglected. But some important features of miniaturized diaphragm pumps, like the back pressure dependent pump yield (V_{yield}), can be understood. In case of low pump frequencies and by neglecting valve leakage, integration of (14) after some steps of calculation leads to:

$$V_{yield}(p_1, p_2) = V_m(p_1, A = A_0) - V_m(p_2, A = 0) - |V_{iv}(p_1 - p_2)| - |V_{ov}(p_1 - p_2)| - |V_{gas}(p_1) - V_{gas}(p_2)| - |V_0(p_1) - V_0(p_2)| \qquad (15)$$

A_0 is the amplitude of the actuation parameter $A(t)$. If the fluid capacitances of the driving diaphragm (C_m), the enclosed gas volume (C_{gas}) and the elastic deformation of the pump chamber housing (C_0) are constant, equation (15) results in:

$$V_{yield}(\Delta p) = V_{yield}(\Delta p = 0) - \left(|C_m^{A=0}| + |C_{gas}| + |C_0|\right)\Delta p - |V_{iv}(-\Delta p)| - |V_{ov}(-\Delta p)| \qquad (16)$$

with $\Delta p = p_2 - p_1 > 0$. It can be seen that the fluid capacitance of the driving diaphragm leads to a

decreasing pump yield with higher back pressure Δp. For the optimization of pump performance also the volume displacement of the microvalves has to be taken into account. It should be noticed that only the volume displacement in the reverse direction of the valves has an influence on the pump yield at low pump frequencies (if valve leakage can be neglected). Thereby the mechanism is equal to the degradation of the pump yield with an enclosed gas bubble (C_{gas}) or an elastic pump housing (C_0). The volume displacement in forward direction does not affect the back pressure dependent pump yield at low frequencies.

So in order to find the best type of microvalve for high pump rates and low back pressure dependence, we have to look for a compromise between low fluid resistance in forward direction, small volume deformation in reverse direction, as well as a good mechanic stability towards shock waves. As can be seen in figure 3, in some cases this is difficult to realize by the use of diaphragm valves.

As the volume stroke of the driving diaphragm is becoming smaller with the outer dimensions of the pump, these effects are getting more and more important, especially for further miniaturization. The until now smallest type of miniaturized diaphragm pump has been an electrostatically driven device with the outer dimensions of $7 \times 7 \times 2$ mm^3 [15]. A maximum hydrostatic pressure of 310 hPa (3100 mm H_2O) and maximum pump rates of 350 μl/min have been reached and reproduced at a supply voltage of 200 V. The total input power is less than 1 mW [14]. Thereby the measured back pressure dependent pump yield is a good verification of equation (15) [14].

5.2. Extended model

An improved simulation of the pump dynamics is possible, if the flow resistance β and the fluid inductivity α of the connected inlet/outlet fluid channels (index i/o) are taken into account (figure 7). In this case the hydrostatic pressures p_i/p_0 on inlet/outlet side of the pump become time dependent.

$$p_i = p_1 - \rho\beta_i\Phi_i - \rho\alpha_i\frac{\mathrm{d}\Phi_i}{\mathrm{d}t}$$
$$p_0 = p_2 + \rho\beta_0\Phi_0 + \rho\alpha_0\frac{\mathrm{d}\Phi_0}{\mathrm{d}t} \qquad (17)$$

The insertion of (8) in (17) results in the basic differential equations for the dynamics of the fluid in the inlet/outlet channel connected with the pump.

$$\alpha_i\rho\frac{\mathrm{d}V_{iv}}{\mathrm{d}p_{iv}}\ddot{p}_{iv} + \alpha_i\rho\frac{\mathrm{d}^2V_{iv}}{\mathrm{d}p_{iv}^2}\dot{p}_{iv}^2 + \left(\beta_i\rho\frac{\mathrm{d}V_{iv}}{\mathrm{d}p_{iv}} + \alpha_i\rho\frac{\mathrm{d}\Phi_{iv}}{\mathrm{d}p_{iv}}\right)\dot{p}_{iv} + \beta_i\rho\Phi_{iv} + p_{iv} - p_1 + p = 0 \qquad (18)$$

$$\alpha_0\rho\frac{\mathrm{d}V_{ov}}{\mathrm{d}p_{ov}}\ddot{p}_{ov} + \alpha_0\rho\frac{\mathrm{d}^2V_{ov}}{\mathrm{d}p_{ov}^2}\dot{p}_{ov}^2 + \left(\beta_0\rho\frac{\mathrm{d}V_{ov}}{\mathrm{d}p_{ov}} + \alpha_0\rho\frac{\mathrm{d}\Phi_{ov}}{\mathrm{d}p_{ov}}\right)\dot{p}_{ov} + \beta_0\rho\Phi_{ov}p_{ov} + p_2 - p = 0 \qquad (19)$$

But also the basic equation for the dynamics of the pump chamber has to be recalculated. With the additionally system components, the degrees of freedom increases and the time dependent hydrostatic pressure differences ($p_{iv} = p_i - p/p_{ov} = p - p_0$) over the passive check valves are now additionally independent variables together with the pump chamber pressure p. This results in:

$$\dot{p} = \frac{\Phi_{iv}(p_{iv}) - \Phi_{ov}(p_{ov}) + \frac{\mathrm{d}V_{iv}}{\mathrm{d}p_{iv}}\dot{p}_{iv} - \frac{\mathrm{d}V_{ov}}{\mathrm{d}p_{ov}}\dot{p}_{ov} - \left.\frac{\partial V_m}{\partial A}\right|_p \frac{\mathrm{d}A}{\mathrm{d}t}}{\left.\frac{\partial V_m}{\partial p}\right|_A - \frac{\mathrm{d}V_{gas}}{\mathrm{d}p} + \frac{\mathrm{d}V_0}{\mathrm{d}p}} \qquad (20)$$

For the evaluation of the dynamics of a miniaturized diaphragm pump in the extended model, a system of 3 coupled non-linear differential equations (18)–(20) has to be solved. In general this can be done only by numerical computation. An analytical solution is possible in one special case, if the volume displacement of the valves can be neglected and all characteristic curves are linear. This will be done later (Channel Design Fields).

To demonstrate the effect of the flow channels connected with the pump, simulations using the basic and the extended model were compared in figure 8. To simplify the detailed description of the different pump components used in the following simulations, all characteristic functions ($\Phi_{iv}(p_{iv})$, $\Phi_{ov}(p_{ov})$, $V_{iv}(p_{iv})$, $V_{ov}(p_{ov})$, $V_m(p, A)$) have been assumed to be linear. Therefore all components can be described by their fluid resistances and fluid capacitances.

The flow resistances of the valves were assumed as $\rho\beta_{iv/ov} = 0.1$ min.hPa/μl (5 min.hPa/μl) in forward (backward) direction, their fluid capacitances as $\rho^{-1}C_{iv/ov} = 0.15$ nl/hPa (0.01 nl/hPa). The fluid capacitance of the driving diaphragm has been calculated with $\rho^{-1}C_m = 0.6$ nl/hPa. The transient behavior of the actuation parameter A (see equation (13)) has been assumed as a square wave with a frequency of 20 Hz and an amplitude A_0 of −200 hPa. The fluid channels, simulated only in the framework of the extended model, have been calculated with a length of 100 mm and a radius of 0.3 mm (circular cross section). For the fluid data, the viscosity and the density of water were used ($\eta = 0.001$ Pa.s, $\rho = 1$ g/cm^3).

In figure 8(a) the transient pump chamber pressure p during the supply mode and the pump mode is depicted. A square wave form for the transient behavior of the actuation parameter has been assumed and, therefore, the pressure changes instantly at the beginning of the supply mode and the pump mode. In figure 8(b) the volume displacement of the inlet valve can be seen. In contrast to the basic model, the displacement of the inlet valve, simulated within the framework of the extended model, cannot change instantly. The reason is that the movement of the valve is coupled with the inertia (inductivity) of that fluid in the inlet tubing. An acceleration time of about 2 ms is needed in order to reach the maximum displacement.

The coupling between the inertia of the fluid mass in the flow channels and the fluid capacitances of the valves and the driving diaphragm leads to a weak oscillation of all quantities depicted in figure 6(a)–(d). The acceleration time for the valve movement and the oscillations of all quantities are typical effects for the influence of flow channels on the dynamics of miniaturized diaphragm pumps. It should be mentioned that there is a drastic difference in the results

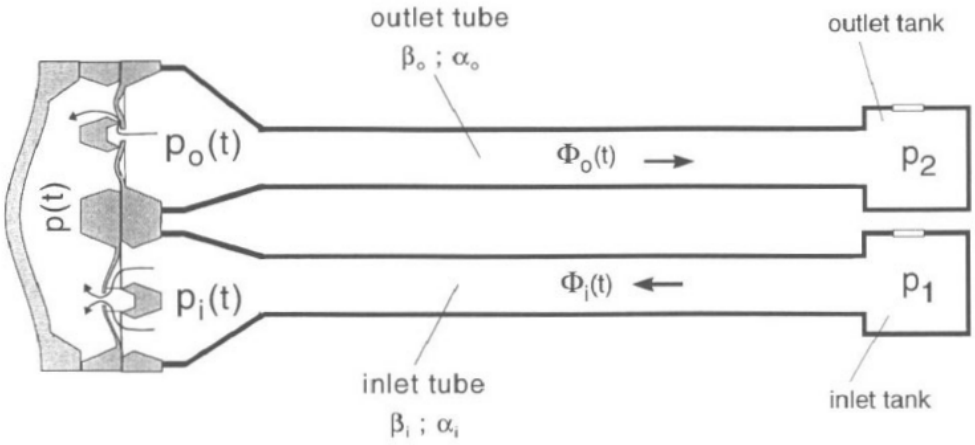

Figure 7. Schematic view of a micropump connected with a peripheral fluid system.

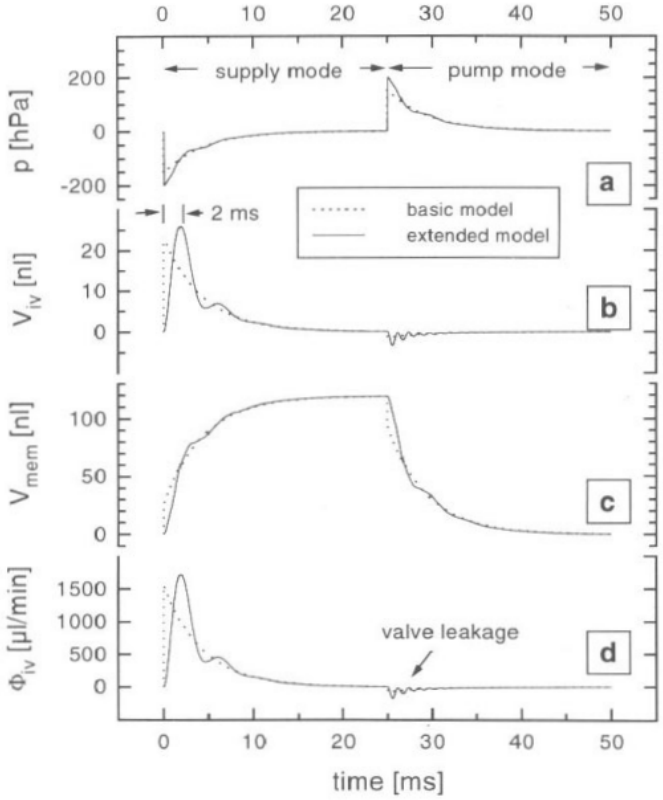

Figure 8. Comparison of transient quantities, simulated with the basic and the extended model ($p_1 = p_2 = 0$ hPa).

between the basic and the extended model, if longer fluid channels are used. This will be demonstrated later, when measurements will be compared with simulations.

6. Pressure smoothing elements (PSEs)

For many applications, the oscillation of pressure and flow in fluid channels has to be suppressed. Analogous to the procedure with macroscopic pumps, the oscillations can be avoided by the use of elastic elements. These elements have to be in contact with the oscillating fluid in the inlet/outlet pipe and are leading to a smoothing of pressure and flow signals. In the macroscopic world an enclosed gas volume is used as an elastic element very often. For microfluid systems, a deflectable diaphragm with a large fluid capacitance is more appropriate than a gas volume.

For this reason, we integrated 'pressure smoothing elements' into the model. According to figure 9, the PSEs were characterized by their volume displacements $V_{ip}(p_{ip})$ and $V_{op}(p_{op})$ (or their fluid capacitances $C_{ip/op}$). For the calculations, the PSEs can be placed anywhere at the inlet or outlet tubing. But for an optimum function, the distance between pump and PSEs should be as small as possible. Using PSEs, the number of differential equations increases. Two new equations of second order are necessary to describe the new independent pressure variables at the smoothing elements (p_{ip} and p_{op}). The procedure for the evaluation of the two new equations is very equal to equation (17) in the case of the extended model and results in the basic differential equations (21)–(25). They describe the dynamics of a miniaturized diaphragm pump connected with a peripheral fluid system via two pressure smoothing elements:

dynamics of pump chamber:

$$\left(\frac{dV_m}{dp}+\frac{dV_0}{dp}\right)\dot{p} = \Phi_{iv}-\Phi_{ov}+\frac{dV_{iv}}{dp_{iv}}\dot{p}_{iv} + \frac{dV_{ov}}{dp_{ov}}\dot{p}_{ov}-\left.\frac{\partial V_m}{\partial A}\right|_p \dot{A} \tag{21}$$

dynamics of inlet fluid channel:

$$\rho\alpha_{ip}\frac{dV_{iv}}{dp_{iv}}\ddot{p}_{iv} = p_{ip}-p_{iv}-p-\rho\alpha_{ip}\frac{d^2V_{iv}}{dp_{iv}^2}\dot{p}_{iv}^2 - \rho\left(\frac{d\Phi_{iv}}{dp_{iv}}+\beta_{ip}\frac{dV_{iv}}{dp_{iv}}\right)\dot{p}_{iv}-\rho\beta_{ip}\Phi_{iv} \tag{22}$$

dynamics of outlet fluid channel:

$$\rho\alpha_{op}\frac{dV_{ov}}{dp_{ov}}\ddot{p}_{ov} = -p_{op}-p_{ov}+p-\rho\alpha_{op}\frac{d^2V_{ov}}{dp_{ov}^2}\dot{p}_{ov}^2 - \rho\left(\alpha_{op}\frac{d\Phi_{ov}}{dp_{ov}}+\beta_{op}\frac{dV_{ov}}{dp_{ov}}\right)\dot{p}_{ov}-\rho\beta_{op}\Phi_{ov} \tag{23}$$

dynamics of inlet fluid channel between pump and PSE:

$$\rho\alpha_i\frac{dV_{ip}}{dp_{ip}}\ddot{p}_{op} = -\frac{\alpha_i}{\alpha_{ip}}(p+p_{iv})+\left(1+\frac{\alpha_t}{\alpha_{ip}}\right)p_{ip}$$

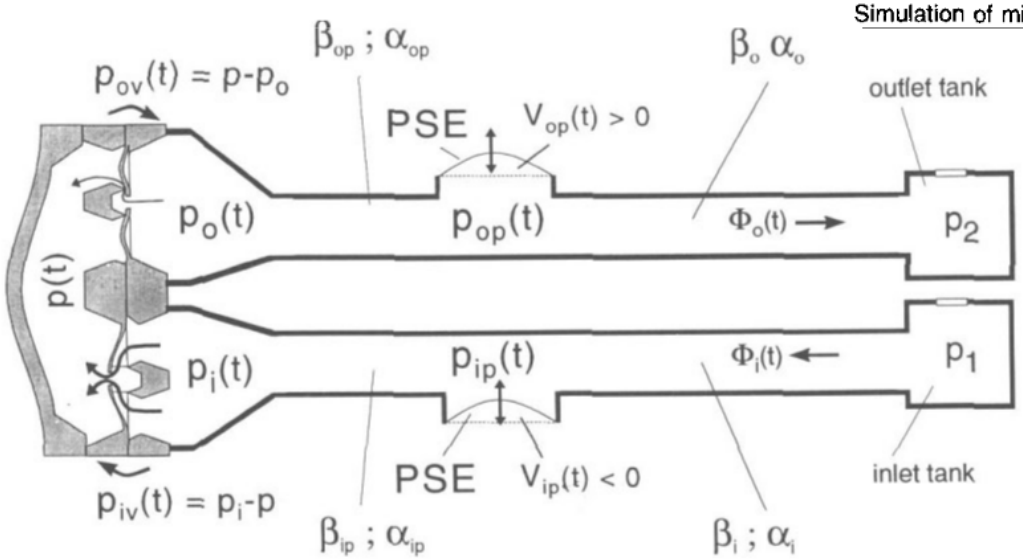

Figure 9. Schematic view of a micropump connected with the peripheral fluid system via PSEs in order to smooth the flow pulsation in fluid channels.

$$+\rho\beta_i\frac{d^2V_{ip}}{dp_{ip}^2}\dot{p}_{ip}^2-\rho\left(\frac{\alpha_i}{\alpha_{ip}}\beta_{ip}-\beta_i\right)\frac{dV_{iv}}{dp_{iv}}\dot{p}_{iv}$$
$$+\beta\frac{dVip}{dp_{ip}}\dot{p}_{ip}+\rho\left(\beta_i-\frac{\alpha_i}{\alpha_{ip}}\beta_{ip}\right)\Phi_{iv}-p_1 \qquad (24)$$

dynamics of outlet fluid channel between pump and PSE:

$$\rho\alpha_0\frac{dV_{op}}{dp_{op}}\ddot{p}_{op}=-\frac{\alpha_0}{\alpha_{op}}(p-p_{ov})+\left(1+\frac{\alpha_0}{\alpha_{op}}\right)p_{op}$$
$$+\rho\beta_o\frac{d^2V_{op}}{dp_{op}^2}\dot{p}_{op}^2+\rho\left(\frac{\alpha_o}{\alpha_{op}}\beta_{op}-\beta_o\right)\frac{dV_{ov}}{dp_{ov}}\dot{p}_{ov}$$
$$+\beta_o\frac{dV_{op}}{dp_{op}}\dot{p}_{op}+\rho\left(\frac{\alpha_o}{\alpha_{op}}\beta_{op}-\beta_o\right)\Phi_{ov}-p_2. \qquad (25)$$

Simulations with and without PSEs are depicted in figure 10. For these experiments an electrostatically actuated diaphragm pump with a supply voltage of 150 V and an operation frequency of 100 Hz was used (see figure 6). The characteristic curves of the microvalves are depicted in figure 3 (flap valves). The total length and the radius of the flow channels were set to 100 mm and 0.3 mm respectively at the inlet/outlet side of the pump. In the case of simulations with PSEs, elastic elements with a fluid capacitance of $\rho^{-1}C_{ip/op} = 10$ nl/hPa were placed at a distance of 5 mm to the valves.

The time dependent pump chamber pressure, p, the pressures $p_{i/o}$ in the flow channels and the transient flow rates $\Phi_{i/o}$ in the channels were simulated in the extended model without PSEs and are depicted on the left side of figure 10. These transient trajectories can be compared with the equivalent curves, achieved by simulations including PSEs, on the right side of figure 10. The first 10 operation cycles (supply mode and pump mode) were plotted in order to illustrate the starting characteristics when switching on the supply voltage.

It can be seen that pressure amplitudes in flow channels can be smoothed from some hundreds of hPa without PSEs to less than ±10 hPa by the use of PSEs. Very important is the smoothing of the transient flow rates. The high frequency flow oscillation with amplitudes between −4000 µl/min and +10000 µl/min can be smoothed to nearly continuous flow of about 400 µl/min. Furthermore, it can be seen that after some cycles of operation (50 ms) the flow signal in the tubing gets periodical and starting effects disappear. It should be mentioned that flow channels with elastic walls (for example silicon tubes) lead to similar effects. In this case the theoretical description is nevertheless much more complicated than demonstrated with PSEs. The reason is that the fluid capacitance of these tubes is distributed to the whole channel length.

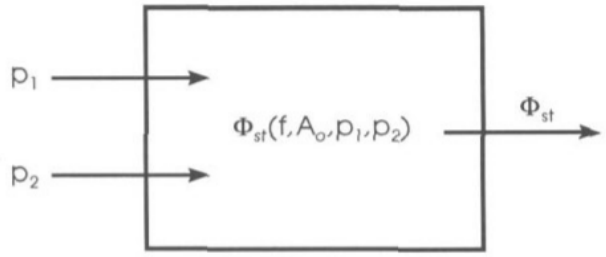

Figure 11. A miniaturized diaphragm pump, handled as a black box in the fluid system.

From figure 10 it is quite obvious that it is possible to decouple the dynamic interaction between miniaturized diaphragm pumps and the surrounding fluid system by the use of elastic elements. This is of large importance for the simulation of more complex fluid systems, consisting of several micropumps, flow channels and other elements. By neglecting the small oscillations in fluid flow and pressure behind the PSEs, it is possible to describe the pump yield of a miniaturized diaphragm pump with a static function:

$$\Phi_{st} = \Phi_{st}(f,\ A_0,\ p_1,\ p_2) \qquad (26)$$

It depends on the operation parameters (f, A_0) as well as on the system pressures (p_1, p_2) and is not explicitly time dependent. By use of this function, the pump in a fluid network can be handled as a black box. The input parameters for the black box are the two system pressures p_1 and p_2 at the nodes to the fluid network and the output parameter is the flow rate Φ_{st} (figure 11).

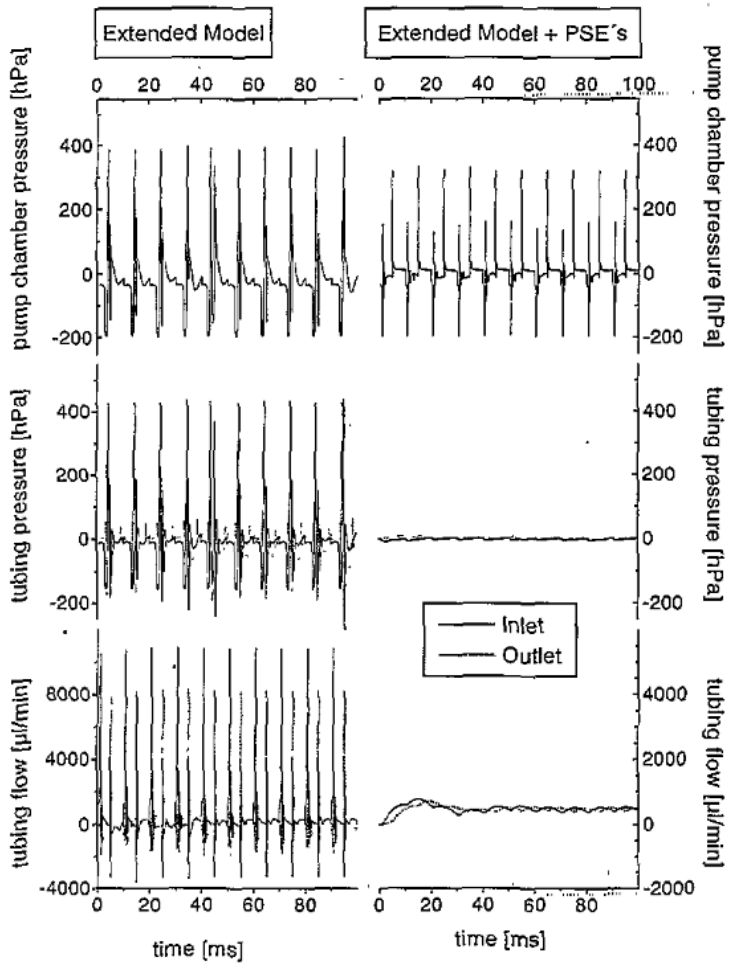

Figure 10. Transient simulation: influence of PSEs on pressure and volume flow in fluid channels (frequency 100 Hz, supply voltage 150 V, tubing length 100 mm, radius 0.3 mm).

7. Microfluid networks

In the previous sections, the static and dynamic behavior of some basic fluid elements of microfluid systems have been discussed. The next step is to contribute these elements to functional microfluid networks. In the macroscopic world, there are many simulation tools available to calculate the behavior of networks. A software tool called DSH (digital simulation of hydraulic systems) has been developed at the RWTH University of Aachen, Germany [17]. From the fluid power center of the University Bath, UK, a tool called BATHfp is available [18]. With these tools, the layout of hydraulic systems can be created, using a graphic interface. The fluid system can include a lot of channels, valves, restrictions, branchings, macroscopic pumps and other hydraulic elements. The elements are described by characteristic functions which can be loaded from a library.

As dynamics of miniaturized diaphragm pumps differ very much from macroscopic pumps, micropumps have not been available as library elements until now. However, the calculation of characteristic functions Φ_{st} of different types of miniaturized diaphragm pumps can be performed with special tools (for example PUSI, discussed in the next section) and so micropumps can be added to the libraries. So a sophisticated optimization of the pump performance can be achieved by use of these dedicated tools. Performance simulation of the whole fluid system (for example a complex chemical analysis system) can be calculated with conventional tools, known from the macroscopic world and using miniaturized diaphragm pumps as black box elements.

8. Simulation tool PUSI

Miniaturized diaphragm pumps will be very important sub-systems of microfluid networks in the future. The performance simulation of these pumps is quite difficult, because there is a strong interaction between the pump dynamics and the peripheral fluid system as has been shown before. Furthermore, the characteristics of the pump elements, the volume displacement characteristic and the flow characteristic of the valves, as well as—in some cases—the actuation characteristic $V_m(p, A)$ are strongly non-linear. Thus the simulation of the miniaturized diaphragm pumps is not possible or at least quite difficult by standard hydraulic tools from the macroscopic world.

For this reason, we developed a numerical simulation tool PUSI, which runs on a PC-system under Microsoft Windows. By the use of PUSI, the numerical evaluation of the pump dynamics in the extended model (including PSEs) is possible. Special numerical and physical problems combined with highly non-linear characteristic functions

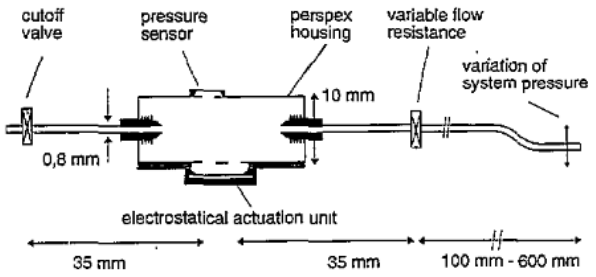

Figure 12. Experimental setup for transient pressure measurements.

and singularities have been taken into account. A large set of library functions is available in order to characterize the different components of diaphragm pumps. Additions to the library are possible in an easy way by fitting theoretical or experimental data with user defined functions. Effects from varying experimental parameters (actuation frequency, pressure p_1, p_2, ...) and design parameters (different actuation mechanisms, flow characteristic and volume deformation of microvalves in forward and reverse direction, fluid capacitances of pump chamber housing and PSEs) can be calculated in the framework of the different models introduced before (basic, extended, extended including PSEs). Simulations can be done, either by calculating only one or more operation cycles at a fixed parameter set (leading to the transient behavior of the specified layout of the pump), or by varying one to two experimental parameters (leading for example to the characteristic function $\Phi_{st}(p_1, p_2)$), A special graphic part of the program allows a comfortable comparison of simulations with experimental results.

9. Comparison between measurements and simulations

In order to test the validity of the theoretical model, transient pressure measurements were carried out. The experimental setup is given in figure 12. Electrostatic or pneumatic actuation units, as well as a miniaturized pressure sensor were fitted in a perspex housing [14, 15]. For pressure measurements, the deflection of a 800 μm wide and 0.4 μm thick silicon carbide diaphragm was detected by an optical measurement system with a time resolution of 0.4 ms. In order to study the effect of different flow characteristics, the micro valves were substituted by a variable flow resistance.

The transient pressure signals in the case of electrostatic actuation are compared with simulations in the framework of the extended model in figure 13. At a high fluid resistance of the variable flow restriction ($\rho\beta$ = 1.25 hPa.min/μl), there is no influence of the peripheral fluid system (figure 13(a) and (b)). The signals during supply mode and pump mode are not symmetrical which is typical of electrostatic actuation. In addition, a shoulder in the transient signal of the supply mode (figure 13(b)) is a characteristic feature of an electrostatically actuated diaphragm pump in some special parameter constellations. At low fluid resistance of the variable flow restriction ($\rho\beta$ = 0.05 min.hPa/μl) the signals are dominated by oscillations

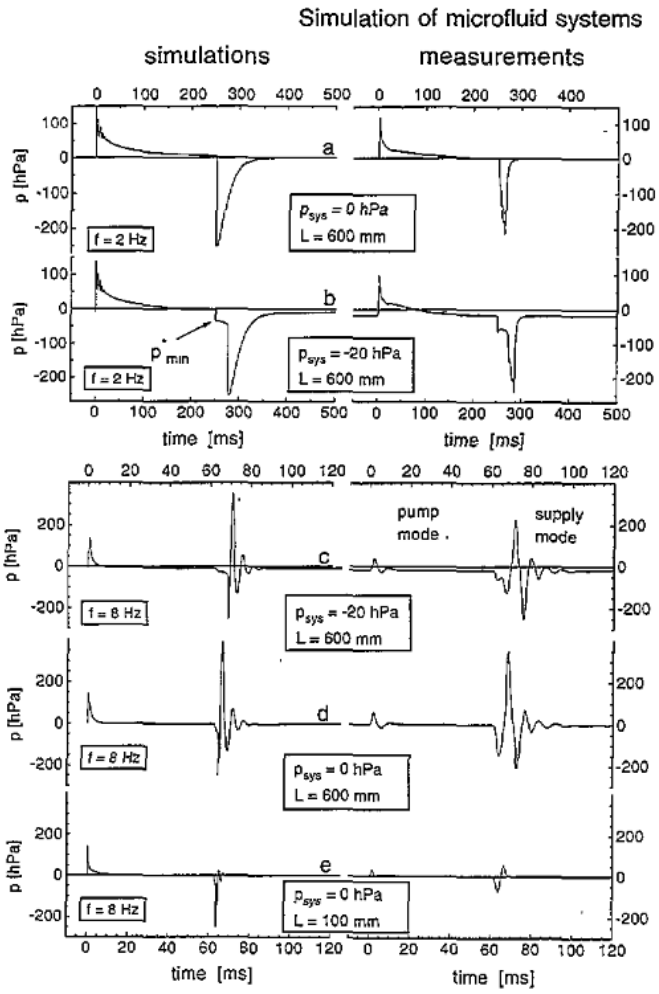

Figure 13. *Transient measurements and simulations using an electrostatically driven actuation unit (tube radius: 0.4 mm).*

of the fluid in the tube (figure 13(c) and (d)). The small deviations between measurements and simulations are due to the inertia of the fluid *inside* the pump chamber. This effect was not simulated in the extended theoretical model and is only important because the pump chamber volume is quite large in the special housing for this experiment. By reducing the tubing length from 600 mm to 100 mm, the effects from the peripheral fluid system become less important (figure 13(e), see also figure 8).

The transient signals in the case of pneumatic actuation are depicted in figure 14. They demonstrate that the inertia of fluid has to be taken into account, whenever the pneumatic time constants for turning on/off the actuation forces are of the same order as the time constants combined with the inductivity of the fluid channels. In figure 14 the driving diaphragm was actuated by a pneumatic pressure with an amplitude of 200 hPa, generated by an external pneumatic system. The time constants for pneumatic actuation in the supply/pump mode were 3.5/8.0 ms. At a high fluid resistance of the flow restriction ($\rho\beta$ = 0.625 min.hPa/μl) there is no influence of the peripheral system (figure 14(a)). In contrast, at a low fluid resistance ($\rho\beta$ = 0.033 min.hPa/μl), oscillations of the pressure signal can be seen. The inertia effects are more important for short time constants. This can be seen by comparing the transient signals of supply mode (3.5 ms) and pump mode (8 ms) (figure 14(b)).

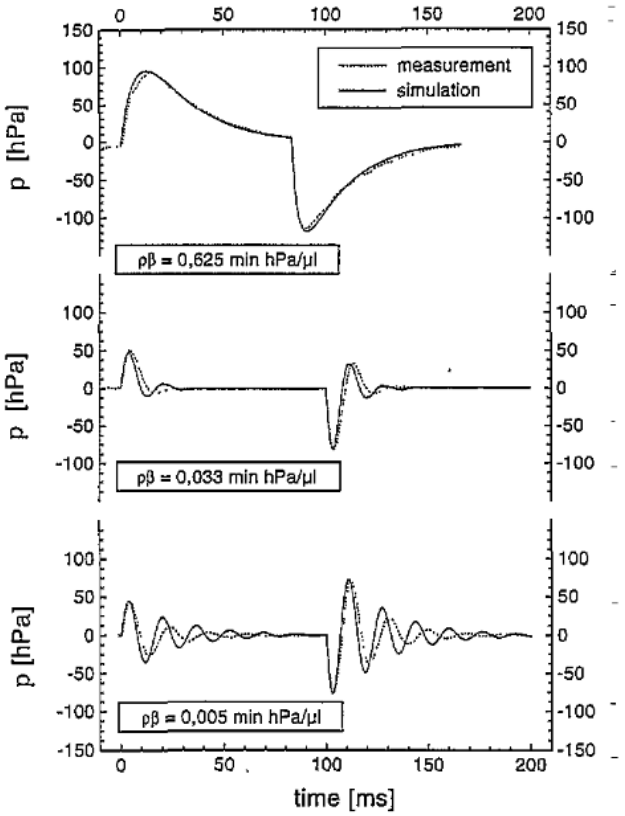

Figure 14. Transient measurements using a pneumatically driven actuation unit (tube radius: 0.4 mm; tube length: 600 mm).

There were two reasons why we substituted the passive check valves in the experimental setup by simple flow restrictions: First, the basic interaction between the dynamics of the pump diaphragm and the peripheral fluid system could be demonstrated in dependence on different flow resistances of *microvalves* within one simple experimental setup. Second, we wanted to use a constant, pressure independent flow resistance, in order to compare the results with an analytical solution of the extended model of the pump dynamics, which is only possible if all functions are linear. This will be demonstrated in the next section and leads to a channel design field, from which it is easy to see, whether the dynamics of a special configuration is influenced by the peripheral fluid system or not.

Finally it should be mentioned that also transient measurements in miniaturized diaphragm pumps with two passive check valves were carried out. Three pressure sensors were used in order to detect the pump chamber pressure p as well as the pressures p_i and p_o outside the pump chamber. These experiments also show good agreement compared with simulations [16].

10. Channel design fields

The dynamics of the experimental setup, depicted in figure 12, can be calculated analytically for linear characteristic functions (constant fluid capacitance of driving diaphragm (see figure 5(b), constant fluid resistance of the microvalves, no fluid capacitances of microvalves). These demands were fulfilled by the measurements depicted in figure 14, which have been recorded using a pneumatically driven actuation unit. In this example, the actuation parameter A equals the pneumatic actuation pressure $p_a(t)$, which is depicted in figure 5(c) ($A(t) = A_0 \exp(-t/\tau_a) = P_{ao} \exp(-t/\tau_a)$.

In the following, $p_1 = p_2 = 0$ hPa as well as $p(t = 0) = 0$ hPa (atmospheric pressure) were assumed. Solving the differential equation system under these conditions in the extended model, the transient pressure drop p_{iv} over the flow restriction during the supply mode of the pump equals:

$$p_{iv}(t) = \frac{p_{a0}\beta_{iv}}{\alpha_i(s_1 - s_2)}\left(\frac{\lambda}{s_2 + \lambda}\exp(s_2 t) - \frac{\lambda}{s_1 + \lambda}\exp(s_1 t) - \frac{\lambda(s_1 - s_2)}{(s_2 + \lambda)(s_1 + \lambda)}\exp(-\lambda t)\right) \tag{27}$$

with the abbreviation $\lambda = 1/\tau_a$ and the frequencies s_1 and s_2, defined as:

$$s_{1/2} = -\frac{\beta_{iv} + \beta_i}{2\alpha_i} \pm \sqrt{\left(\frac{\beta_{iv} + \beta_i}{2\alpha_i}\right)^2 - \frac{1}{\alpha_i C_m}} \tag{28}$$

For physical reasons, the coefficients C_m, β_{iv}, α_i, β_i and τ_a are positive in any case. Thus the real parts of s_1 and s_2 are negative and there is always a damping of the pressure. If s_1 and s_2 have a complex part, the transient pressure $p(t)$ and $p_{iv}(t)$ have an oscillating characteristic. This is synonymous with:

$$\left(\frac{\beta_{iv} + \beta_i}{2\alpha_i}\right)^2 - \frac{1}{\alpha_i C} < 0 \tag{29}$$

The discussion of the relation leads to a criterion: If the relation

$$C_m > \frac{\rho A_\square}{8\pi\eta\gamma_{iv}} \tag{30}$$

is valid, then no oscillating solutions occur independent of channel length L. Otherwise there are two critical lengths L_- and $L_+ > 0$.

$$L_{+/-} = \frac{2A_\square^2\rho(\rho A_\square - 4\pi\eta\beta_{iv}C_m \pm \sqrt{\rho A_\square(\rho A_\square - 8\pi\eta\beta_{iv}C_m)})}{C_m(8\pi\eta)^2} \tag{31}$$

If the length L of the channel is between L_- and L_+, then the pressures $p(t)$ and $p_{iv}(t)$ are oscillating. In this case there is a strong interaction between the dynamics of the micropump and the inductance of the fluid channels. Considering a diagram channel length L versus the fluid conductance $1/(\rho\beta_{iv})$ of the restriction, the curves L_+ and L_- define an area, where this interaction occurs. In figure 15 this area is depicted for a constant fluid capacitance ($\rho^{-1}C_m = 0.5$ nl/hPa) of the driving diaphragm and a constant cross section $A_\square$. This field can be compared with the transient pressure measurements at different tubing lengths L and different fluid resistances β_{iv} of the flow restriction. The measurements completely agree with the prediction of the design field.

The characteristic lengths L_+ and L_- evaluated for three different channel radii (R = 100 μm, R = 200 μm, R = 400 μm) are depicted in figure 16. There are three areas where different quantities dominate the dynamics of the pump. In the case of small fluid conductance of the

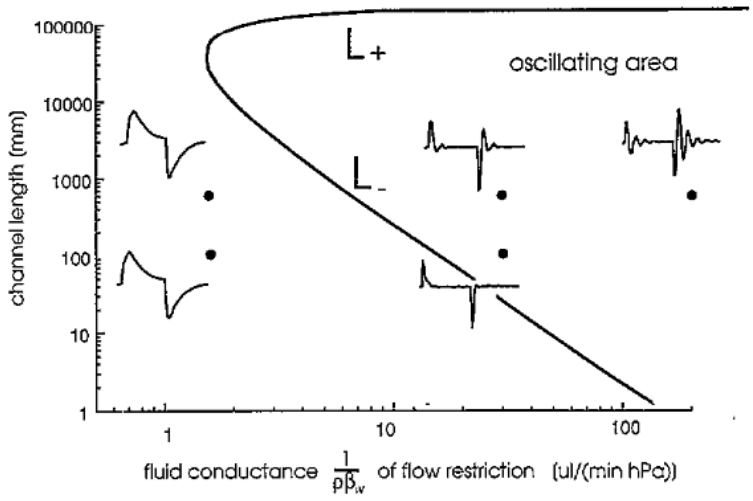

Figure 15. Design field for miniaturized diaphragm pumps, showing different types of dynamic behaviour (fixed tubing radius 0.4 mm).

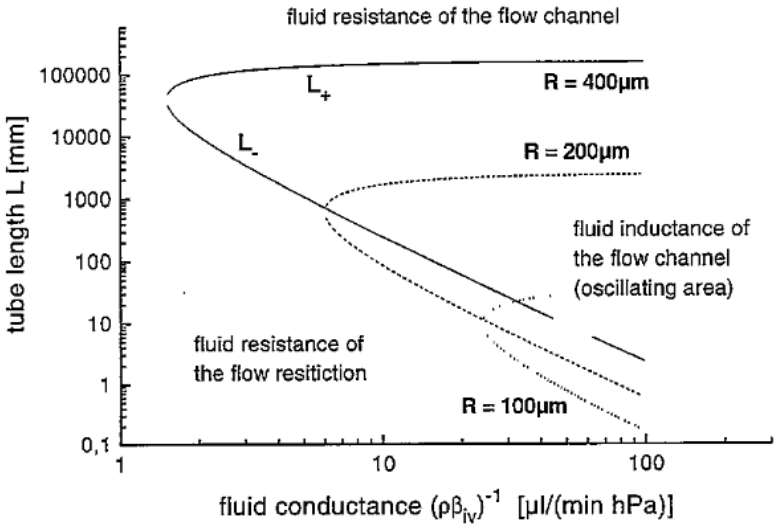

Figure 16. Channel design field (parameter: tube radius).

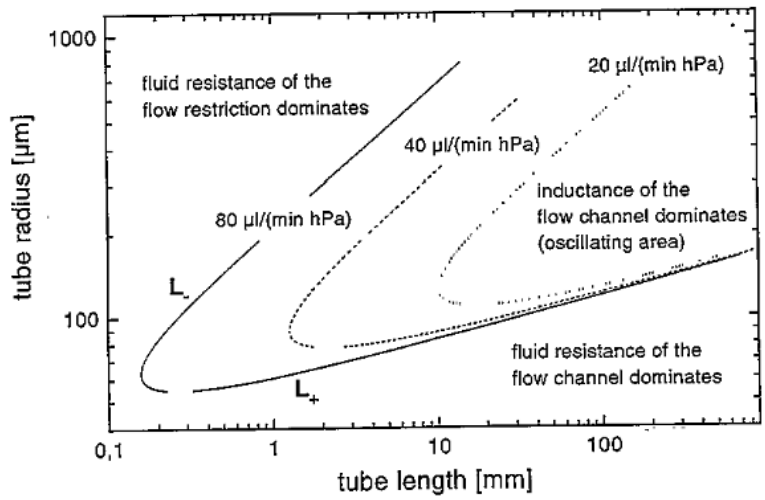

Figure 17. Channel design field (parameter: fluid conductance $(\rho\beta_{iv})^{-1}$ of the flow restriction).

flow restriction (high fluid resistance) this fluid resistance dominates the dynamics of the pump. Only for very long tube length L the fluid resistance of the tube has the biggest influence on the dynamics of the pump. The third area is the oscillating area, where the fluid inductance of the tube dominate the dynamics of the pump. It occurs only at large fluid conductance of the flow restriction.

It should be mentioned that the critical length L_+ depends strongly on the channel radius R. A reduction of the radius R from 400 μm to 100 μm leads to a decrease of the critical length L_+ from 100 000 mm to 50 mm. That means that using a channel radius of 400 μm, the fluid resistance of the tube can be neglected completely. But if the tube radius is fixed to 100 μm, an influence of the fluid resistance of the flow channel on the dynamics of the pump is possible at a large tube length.

Another graphic representation of equation (27) is depicted in figure 17. The critical length L_+ and L_- are shown versus the channel radius R. The fluid conductance $1/(\rho\beta_{iv})$ of the flow restriction is varied as a parameter. From this type of diagram it can be seen, whether there is an influence from the peripheral fluid system on a micropump with a given fluid conductance of the microvalves. It should be noticed that usually the operation modes of miniaturized diaphragm pumps are in the oscillating area and so the interaction of the system periphery and the micropumps cannot be neglected.

11. Conclusions

In this paper we investigated the properties and the dynamic behavior of different components in microfluid systems (flow channels, microvalves, elastic elements, diaphragm pumps). As has been shown, miniaturized diaphragm pumps are important but complex subsystems of microfluid networks. There is a strong feedback effect caused by the inductivity of flow channels of the fluid system to the dynamics of the pump.

If miniaturized diaphragm pumps are combined with elastic elements (PSEs) the strong interaction between the pumps and the fluid systems can be decoupled and the micropumps can be considered as black boxes. A sophisticated optimization of these pump elements can be achieved, using special numerical tools like PUSI. For the performance simulation of complex fluid systems with variable geometry and including several micropumps, conventional hydraulic simulation tools, known from the macroscopic world, can be used.

References

[1] Cammann C, Lemka U, Rohen A, Sander J, Wilken H and Winter B 1991 Chemo- und Biosensoren - Grundlagen und Anwendungen *Angewandte Chemie* **5** 519–41

[2] Gravesen P, Branebjerg J and Jensen O S 1993 Microfluidics *J. Micromech. Microeng.* **3** 168–82

[3] Shoji S and Esashi M 1994 Micro flow devices and systems *J. Micromech. Microeng.* Microfluids special

[4] Gass V, van de Schoot B H, Jeanneret S and De Rooij N F 1993 Integrated flow-regulated silicon micropumps *Proc. Transducer '93 (Yokohama, 7–10 June 1993)* pp 1048–51

[5] Lammerink T S J, Elwenspoek M and Fluitman J H J 1993 Integrated micro-liquid dosing system *Proc. MEMS '93 Workshop (Fort Lauderdale, FL, 7–19 February 1993)* pp 254–9

[6] van der Schoot B H, Jeanneret S, van den Berg A and de Rooij N F 1993 Modular setup for a miniaturized chemical analysis system *Sensors Actuators* **B15–B16** 211–3

[7] Melcher K 1972 *Ein Reibungsmodell zur Berechnung von Instationären Strömungen in Rohrleitungen an Brennkraftmaschinen* Habitilationsschrift Robert Bosch GmbH

[8] Harley J, Bau H, Zemel J N and Dominko V 1989 Fluid flow in micron and submicron size channels *Proc. MEMS 1989 (Salt Lake City, 20–22 February 1989)* pp 25–8

[9] Pfahler J, Harley J, Bau H and Zemel J 1990 Liquid transport in micron and submicron channels *Sensors Actuators* **A21–A23** 431–4

[10] Schädel H M 1979 *Fluidische Bauelemente und Netzwerke* Vieweg Verlag, Braunschweig

[11] Timoshenko S and Krieger S W 1959 *Theory of Plates and Shells* (New York: McGraw Hill)

[12] van de Pol F C M 1989 A pump based on micro engineered techniques *PhD Thesis* University of Twente, Netherlands

[13] Zengerle R, Richter M, Brosinger F, Richer A and Sandmaier H 1993 Performance simulation of microminiaturized membrane pumps *Proc. Transducer '93 (Yokohama, 7–10 June 1993)* pp 106–9

[14] Zengerle R 1994 Mikro-Membranpumpen als Komponenten für Mikro-Fluidsysteme *PhD Thesis* Verlag Shaker, Aachen ISBN: 3-8265-0216-7

[15] Zengerle R, Geiger W, Richter M, Ulrich J, Kluge S and Richter A 1994 Application of micro diaphragm pumps in microfluid systems *Proc. Actuator '94 (Bremen, 15–17 June 1994)* pp 25–9

[16] Zengerle R, Geiger W, Richter M, Ulrich J, Kluge S and Richter A 1994 Transient measurements on miniaturized diaphragm pumps in microfluid systems *Proc. Eurosensors '94 (Toulouse, 25–28 September 1994)*

[17] 1992 DSH (digital simulation of hydraulic systems); Institut für hydraulische und pneumatische Antriebe und Steuerungen; RWTH Aachen, Germany

[18] BATH*fp* 1992 *Interactive Simulation Tool for Dynamic System Analysis* Fluid Power Center, University of Bath